Combined evaluation of myocardial perfusion and coronary morphology in the identification of subclinical CAD

Radiation exposure of ^{13}N-ammonia PET/CT

G. Vincenti[1]; A. Quercioli[1]; H. Zaidi[2]; R. Nkoulou[1]; S. Dewarrat[2]; O. Rager[2]; G. Ambrosio[3]; Y. Seimbille[2]; F. Mach[1]; O. Ratib[2]; T. H. Schindler[1]

[1]Department of Internal Medicine, Cardiovascular Center, Nuclear Cardiology, University Hospital of Geneva, Switzerland; [2]Department of Radiology, Division of Nuclear Medicine, University Hospital of Geneva, Switzerland; [3]Division of Cardiology, University Hospital of Perugia, Italy

Keywords

Low dose, computed tomography coronary angiography, coronary circulation, feasibility, myocardial blood flow, retrospective gating, positron emission tomography

Summary

Purpose: To evaluate the mean effective radiation dose of ^{13}N-ammonia PET/CT and ECG-pulsing CT angiography (CTA) in the evaluation of myocardial perfusion, myocardial blood flow (MBF) and coronary morphology for the identification of subclinical CAD. Patients, material, methods: Following rest-stress ^{13}N-ammonia PET/CT perfusion imaging and MBF quantification, ECG-pulsing CTA at a pulse window of 70% of the R-R cycle was performed in ten healthy controls and in sixteen individuals with cardiovascular risk factors. Individual radiation dose exposure for ECG-pulsing CTA was estimated from the dose-length product. Results: PET demonstrated normal perfusion in all study individuals, while hyperemic MBFs during dipyridamole stimulation and the myocardial flow reserve (MFR) in cardiovascular risk individuals were significantly lower than in healthy controls (1.34±0.26 vs. 2.28±0.47 ml/g/min and 1.48±0.39 vs. 3.24±0.81, both p≤0.0001). Further, ECG-pulsing CTA identified mild calcified and non-calcified coronary plaque burden in 7 (43%) individuals of the cardiovascular risk group. Rest-stress ^{13}N-ammonia PET/CT perfusion study yielded a mean effective radiation dose of 3.07±0.06 mSv (2.07±0.06 mSv from the rest-stress ^{13}N-ammonia injections and 1.0 mSv from the 2 CT transmission scans), while ECG-pulsing CTA was associated with 5.57±2.00 mSv. The mean effective radiation dose of the combined ^{13}N-ammonia PET/CT and ECG-pulsing CTA exams in the evaluation of myocardial perfusion and coronary morphology was 8.0±1.5 mSv. Conclusion: ^{13}N-ammonia PET/CT and ECG-pulsing CTA affords cardiac hybrid imaging studies in the evaluation of subclinical CAD with a relatively low mean effective radiation exposure of 8.0±1.5mSv.

Schlüsselwörter

CT-Angiographie, Koronarkalk, Hybridbildgebung, Myokardperfusion, myokardiale Flussreserve, ^{13}N-Ammoniak, PET-CT, Strahlenbelastung

Zusammenfassung

Ziel: Erfassung der mittleren effektiven Strahlendosis bei kombinierter Anwendung der kardialen ^{13}N-Ammoniak PET/CT und EKG-getriggerten CT-Angiographie (CTA) zur Bestimmung der myokardialen Perfusion, des myokardialen Blutflusses (MBF), und der koronaren Morphologie für die Identifizierung einer subklinischen koronarer Herzerkrankung (KHK). Patienten, Methoden: Bei 10 Gesunden (Kontrollen) und 16 Personen mit kardiovaskulären Risikofaktoren wurde im Anschluss einer Ruhe-Stress-^{13}N-Ammoniak-PET/CT-Perfusions- und MBF-Untersuchung, eine EKG-getriggerte CTA mit einem Trigger-Fenster von 70% des R-R-Zyklus durchgeführt. Die individuelle Strahlendosis-Exposition für die EKG-getriggerte CTA wurde mittels Dosis-Längen-Produkt ermittelt. Ergebnisse: Die PET-Untersuchung ermittelte bei allen Personen eine normale myokardiale Perfusion, wohingegen der hyperämische MBF-Anstieg während Dipyridamol-Stimulation und die myokardiale Flussreserve (MFR) in der kardiovaskulären Risiko-Gruppe im Vergleich zu Kontrollen deutlich vermindert waren (1,34±0,26 vs. 2,28±0,47 ml/g/min und 1,48±0,39 vs. 3,24±0,81, beide p≤0,0001). Des Weiteren wurden mittels EKG-getriggerte CTA kalzifizierte und nicht-kalzifizierte koronare Plaque-Bildung in 7 (43%) der kardiovaskulären Risko-Gruppe identifiziert. Die Ruhe-Stress-^{13}N-Ammoniak-PET/CT-Untersuchung ergab eine mittlere effektive Strahlendosis von 3,07±0,06 mSv (2,07±0,06 mSv von den Ruhe-Stress ^{13}N-Ammoniak Injektionen und 1,0 mSv von den 2 CT Transmissions-Scans), während die EKG-getriggerte CTA mit eine Strahlenbelastung von 5,57±2,00 mSv assoziiert war. Die kombinierte Anwendung einer kardialen ^{13}N-Ammoniak-PET/CT und EKG-getriggerten CTA zur Bestimmung der myokardialen Perfusion und der koronaren Morphologie ergab schlussendlich eine mittlere effektive Strahlendosis von 8.0±1.5 mSv. Schlussfolgerung: Die kombinierte Anwendung einer kardialen ^{13}N-Ammoniak PET/CT und EKG-getriggerten CTA erlaubt kardiale Hybrid-Untersuchungen für die Identifizierung einer subklinischen KHK mit relativ geringer mittlerer effektiver Strahlenbelastung von 8.0±1.5 mSv.

Correspondence to:
Thomas Schindler, MD, PhD
Department of Internal Medicine, Cardiovascular Center, 6th Floor, Nuclear Cardiology
University Hospitals of Geneva
Rue Gabrielle-Perret-Gentil 4
1211 Geneva, Switzerland
E-mail: thomas.schindler@hcuge.ch

Kombinierte Untersuchung der myokardialen Perfusion und koronaren Morphologie für die Identifizierung einer subklinischen koronarer Herzerkrankung (KHK) – Strahlenexposition der kardialen ^{13}N-Ammoniak-PET/CT-Untersuchung
Nuklearmedizin 2010; 49: 173–182
doi: 10.3413/nukmed-0312
received: April 23, 2010
accepted in revised form: July 3, 2010
prepublished online: July 22, 2010

Hybrid positron emission tomography and computed tomography (PET/CT) systems may afford the non-invasive and integrative evaluation of both myocardial perfusion and coronary morphology in individuals at risk for the development of CAD (1, 2). The possibility of PET imaging in concert with tracer kinetic modelling enables a non-invasive quantification of myocardial blood flow (MBF), that may identify reduced hyperemic MBFs or MFR as functional precursor of early stages of developing CAD (3–5). Vice versa, CT-angiography may unmask subclinical non-calcified or calcified coronary plaque burden (6). In particular, the identification and characterization of subclinical stages of the CAD process also carries important prognostic information with increasing clinical interest (7, 8). As regards the radiation exposure ^{13}N-ammonia PET/CT rest-stress perfusion imaging, it may be associated with a radiation dose of about 3–4 mSv (2× ^{13}N-ammonia ≈2–3 mSv and 2× CT-attenuation correction ≈1 mSv). Conversely, the use of conventional helical CTA protocols may expose patients up to 15–25 mSv.

Thus, the radiation exposure especially from CTA has remained a major concern that limited a more widespread use of CTA alone or of hybrid cardiac PET/CT examinations.

For this reason, different strategies to reduce the radiation exposure during CTA have been proposed such as an individual adjustment of the scan length, tube current modulation based on patient's size, a reduced tube voltage of 100 kV, or a combined used of these dose-saving strategies, which has resulted in an efficacious reduction of overall radiation exposure (9). Technological MDCT advancements have put forth in principle two algorithms for a substantial reduction in radiation dose during CTA, such as a sequential scanning with prospective ECG triggering (referred to as "step-and-shoot") (10) or the tube current modulation according to the ECG during a spiral scan (referred to as "dose pulsing" or "ECG-pulsing") (9). Regarding the "step-and-shoot" technique, previous experiences documented the feasibility of this low-dose approach with an effective dose of only 1.1–3.0 mSv (10). Similarly, applying the "step-and-shoot" technique for CTA using a hybrid PET/CT system demonstrated an effective mean dose of 5.5 mSv, which compared well to 20.5 mSv of the conventional helical CTA, while CTA images remained of diagnostic quality (1). As mentioned, another promising approach to reduce the radiation exposure during CTA is the modulation of tube current according to the patient's ECG, with the full current in the relevant phase of the heart cycle, usually in mid- to end-diastolic phase (70–75% of R-R cycle for heart rate < 65 bpm) (9). This algorithm lowered the radiation dose to a mean of 9.4 mSv (9). As these technical advancements in the application of CTA with such as the reported "step-and-shoot" or "ECG-pulsing" technique substantially reduce the radiation dose, a more frequent use of hybrid PET/CT system for a comprehensive evaluation of coronary physiology and morphology appears feasible (1, 2, 11).

In this pilot study, we aimed to evaluate the combined feasibility of ^{13}N-ammonia PET/CT perfusion imaging in conjunction with CT angiography using the ECG-dependent dose modulation ("ECG-pulsing"; maximal tube current at a pulse window of 70% of the cardiac R-R cycle) in the evaluation of myocardial perfusion, MBF and coronary morphology with a dedicated hybrid PET/CT system for the identification of subclinical CAD. The mean effective radiation dose of ^{13}N-ammonia PET/CT and ECG-pulsing CTA in evaluation of myocardial perfusion and coronary morphology in a "one-stop" study session was assessed and, in addition, we compared the effective radiation dose and the image quality of ECG-pulsing CTA to conventional helical CTA.

Patients, material, methods

Study population

^{13}N-ammonia PET/CT perfusion imaging in conjunction with CTA using the ECG-dependent dose modulation (ECG-pulsing) was performed in twenty-six individuals using a dedicated 64-slice Biograph HiRez TruePoint PET-CT scanner (Siemens Medical Solutions, Erlangen, Germany) (▶Tab. 1). The study population comprised, sixteen asymptomatic individuals with cardiovascular risk factors such as arterial hypertension, smoking, hypercholesterolemia and type 2 diabetes mellitus, and ten healthy individuals (controls) (▶Tab. 1). These volunteers were recruited by flyers and newspaper advertisement. Individuals with contraindications to iodinated contrast agent, and non-sinus rhythm were not included for CTA. In these study participants undergoing the PET/CT study, the total Framingham risk score (FRS) was assessed by use of the following factors: age, total cholesterol level, high-density lipoprotein cholesterol level, systolic blood pressure, diabetes, and smoking (12). The absolute 10-year risk for total chronic heart disease (CHD) was estimated by Framingham score (CHD risk) (12), which includes a composite of the risk of future angina pectoris, recognized or unrecognized myocardial infarction, unstable angina, and CHD death. In addition, sixteen patients with intermediate-to-high pretest likelihood for CAD, who were examined previously with conventional helical CTA without ECG-pulsing and without PET perfusion imaging, served as comparative group for the evaluation of the radiation exposures between conventional helical and ECG-pulsing CTA. The conventional helical CTA was performed before the ECG-pulsing protocol for CTA was available. The duration of the ^{13}N- ammonia PET/CT and ECG-pulsing CTA exams was »80–90 minutes. The study was approved by the University Hospitals of Geneva Institutional Review Board, and each participant signed the approved informed consent form.

Noninvasive assessment of myocardial perfusion and MBF

Perfusion ^{13}N-ammonia PET/CT imaging constituted the first part of the PET-CT protocol. Following the topogram used to determine the axial field of view and a low dose CT scan (120 kV, 30 mA) for attenuation correction, PET emission data were acquired during shallow breathing. At first, PET imaging at rest started immediately following injection of approximately 500

MBq of ^{13}N-ammonia for a total duration of 18-minute list-mode PET data acquisition. Twenty one dynamic frames of the ungated first 6-min data (12 × 10 s, 3 × 20 s, 6 × 30 s) were reconstructed using iterative normalized attenuation-weighted ordered subsets expectation maximization (NAW-OSEM). The CT-based attenuation correction map was used to reconstruct the emission data. The default parameters used were ordered OSEM with 8 iterations and 4 subsets followed by a post-processing Gaussian filter. Time-activity curves from the first 12 dynamic frames (12 for 10 s each) in conjunction with a two-compartment tracer kinetic model (13) were used to calculate myocardial blood flow (MBF) in ml/g/min with the use of the PMOD software package (version 2.8 PMOD Technologies Ltd., Zurich, Switzerland) (14). Subsequently, 12-min electrocardiography (ECG)-gated PET emission data were acquired with 10 frames per cardiac cycle. The gated PET emission data were used for the analysis of the relative 13N-ammonia uptake of the left-ventricle and, thus, myocardial perfusion was evaluated visually on reoriented short- and long-axis myocardial slices and semiquantitatively on the corresponding polar map from the last static 18 min transaxial PET image. In addition, the gated PET emission data served for the assessment of global left-ventricular function.

Stress PET perfusion imaging was then performed thirty minutes after the end of the rest PET acquisition using the same acquisition protocol. Stress testing was performed with infusion of standard dose of 140 µg/kg/min of dipyridamole over 4 minutes and after an additional 3 minutes at peak effect of pharmacologic vasodilation of the arteriolar vessels, approximately 500 MBq of ^{13}N-ammonia was injected intravenously and acquisition of emission data with PET was started. Following, a post emission CT transmission scan was performed and used for attenuation correction of the stress images. The CT transmission scan was performed again after the stress PET perfusion imaging in order to account for possible changes in cardiac and pulmonary volumes due to dipyridamole-induced hyperemia. Rest-stress PET images were visually checked for accurate alignment with the CT scan used for attenuation correction.

Heart rate, blood pressure, and a 12-lead ECG were recorded continuously during rest-stress PET/CT myocardial perfusion assessment. Regional MBFs during dipyridamole-stimulated hyperemia and at rest were calculated on a polar map for the LAD, LCx and RCA territory. In the absence of stress-induced regional perfusion defects, these regional MBFs from the three major coronary territories were averaged to yield global MBF of the left ventricle. The ratio of hyperemic over resting MBF defined the myocardial flow reserve (MFR=hyperemic MBF/ resting MBF). From the average of heart rate and blood pressure during the first 2 min of each image acquisition, the rate-pressure product (RPP) was determined as an index of cardiac work. To account for interindividual variations in coronary driving pressure, an index of coronary vascular resistance (CVR) was determined as the ratio of mean arterial blood pressure (mmHg) to MBF (ml/g/min).

Assessment of coronary morphology with CT

ECG-pulsing CTA was performed immediately after the end of PET imaging. Metoprolol was administered intravenously (5–20 mg) (Beloc, AstraZeneca) prior to CTA examination to achieve the target heart rate < 65 bpm. Coaching and training of the patient (practice of breath-hold) was performed prior to PET/CTs scanning to avoid breathing artifacts. In addition, all patients received isosorbide dinitrate 2.5 mg sublingual (Isoket spray, Schwarz Pharma) to obtain maximal vasodilation of epicardial artery. For CTA 80 ml of iomeprol (Iomeron 400, Bracco-Altana Pharma) was infused at a flow rate of 5 ml/s followed by 50 ml saline solution into an antecubital vein via an 18-gauge catheter. Bolus tracking was performed after the injection of 20 ml of contrast agent (5 ml/s) by positioning a region of interest (ROI) into the ascending aorta. CTA was performed with the same CT scanner and retrospective gating, using the available tube current modulation tool referred to as "ECG-pulsing". In this direction, maximal tube current or radiation dose was only applied at the pulse window of 70% of the cardiac R-R cycle (ECG-pulsing). Scanning parameters were: 64 × 0.6 mm collimation, gantry rotation time 330 ms, and a pitch of 0.2. Tube voltage and tube current were adapted to the body mass index (BMI) as described previously (10): 100 kV: BMI <25 kg/m^2, 20 kV: BMI ≥25 kg/m^2; and 500 mA: BMI <25 kg/m^2, 550 mA: BMI 25–27.5 kg/m^2, 600 mA: BMI 27.5–30 kg/m^2, 650 mA: BMI >30 kg/m^2. Scanning was performed from below the tracheal bifurcation to the diaphragm. CT coronary angiography images were reconstructed with a slice thickness of 0.6 and 1 mm.

Conversely, conventional helical CTA without ECG-pulsing was performed according to the aforementioned CTA protocol but with following technical parameters: 64 × 0.6 mm collimation, gantry rotation time 330 ms, pitch 0.2, 120 kV, and range of tube current of 867 to 935 mA, depending on patient size. Using retrospective electrocardiographic gating, we performed routinely reconstructions at 25–35% (systole) and 60–80% (diastole) of the R-R cycle. Transaxial images were reconstructed with a slice width of 0.6 and 1.0 mm.

Estimation of CT dose

The effective radiation dose of ECG-pulsing and helical CTA, respectively, was calculated as the product of the dose-length product (DLP) times and a conversion coefficient for the chest (k = 0.017 mSv/mGy × cm) (15). The latter conversion coefficient reflects the mean between male and female models. The radiation dose for ^{13}N-ammonia PET/CT was calculated as ^{13}N-ammonia activity times 2.00E-03 mSv/GBq (16). The radiation exposure of the CT-attenuation correction for the PET rest-stress emission perfusion images was ~0.5 mSV, respectively.

CTA image analysis

Coronary segments were defined according to a modified 16-segment American Heart

Association model (17). The RCA was defined to include segments 1–4, the LM and LAD arteries were defined to include segments 5–10 (and segment 16, intermediate branch, if present) and the LCx artery was defined to include segments 11–15. Only segments with diameter = 1.5 mm were included in the analysis, because the spatial resolution of 64-slice CT was considered insufficient for an accurate evaluation of smaller vessels (10). Segments with diameter < 1.5 mm or anatomical variants were not evaluated. Two readers (1 cardiologist and 1 radiologist) assessed independently the image quality by using a semi-quantitative five-point grading scale, as described previously (10): 1= excellent quality, no motion artifacts; 2 = minor motion artifacts and mild blurring of the segment; 3 = moderate motion artifacts and moderate blurring without structure discontinuity; 4 = severe motion artifacts and doubling or discontinuity in the course of the segment; 5 = image not evaluable. A score ≤3 was considered diagnostic. Segments with a score > 3 were considered not assessable. The segments were evaluated using volume-rendered 3D-reconstruction, curved multiplanar reformatted (MPR) and maximum intensity projection (MIP) 2D-reconstructed images. Using the 2D/3D visualization software Vitrea 2 (Vital images, Inc.). Discrepancy between observers was resolved in a joint reading. Further, for each segment, both presence of atherosclerotic plaque as well as its composition was determined. Atherosclerotic lesions were identified as morphologically significant if the diameter stenosis was ≥ 50%. Plaque lesions below this threshold were classified as mild and non-significant lesions. Plaque composition was graded as non-calcified plaque (plaques having lower density than contrast enhanced lumen), calcified plaque (plaques with high density), and mixed plaques (composition of both non-calcified and calcified plaque burden)(6).

Tab. 1 Characteristics of study population

CTA			ECG-pulsing		conventional helical
			control	at risk	intermediate-to-high probability
age (years)			42±13	64±13*	70±11*
sex (women/men)			2/8	6/10	5/11
body mass index kg/m^2			23±3	28±7	29±10
left-ventricular ejection fraction (%)			58±9	57±11	59±9
hypertension			0	5	9
hypercholesterolaemia			0	6	12
smoking			0	7	8
diabetes mellitus			0	2	3
lipid status	cholesterol (mg/dl)	total	191±29	231±38*	236±29*
		LDL	123±20	137±44	154±31*
		HDL	48±16	44±18	42±12
	triglyceride (mg/dl)		91±50	151±62*	155±51*
	glucose (mg/dl)		93±11	117±20*	120±22*
myocardial blood flow ml/g /min	at rest		0.71±0.09	0.94±0.20*	/
	after dipyridamole		2.28±0.47	1.34±0.26*	/
	myocardial flow reserve		3.24±0.81	1.48±0.39*	/
CVR mmHg/ ml/g /min	at rest		118±21	87±23*	/
	after dipyridamole		37±8	70±32 *	/
haemo-dynamics	rest-HR (bpm)		65±7	69±10	/
	hyperaemia-HR (bpm)		82±7	77±9	/
	rest-SBP (mmHg)		114±11	123±13	/
	hyperaemia-SBP (mmHg)		114±8	114±7	/
	rest rate-pressure product		7330±843	8432±1560	/

*p < 0.05 versus normal controls; LDL: low-density lipoprotein; HDL: high-density lipoprotein; CVR: coronary vascular resistance; HR: heart rate; SBP: systolic blood pressure

Statistical analysis

Data are presented as mean±SD for quantitative and absolute frequencies for qualitative variables. For comparison of differences, appropriate t tests for independent or paired samples were used (Statistical Analysis Software Institute, Cary, NC, USA). Pearson's correlation coefficient (r) and standard error of the estimate (SEE), assuming a linear regression, was calculated to investigate the association between the FRS and hyperemic MBFs. All test procedures were two-tailed, and p ≤ 0.05 was considered statistically significant.

Results

Patients characteristics and CTA findings

As regards the ECG-pulsing CTA in cardiovascular risk patients, four individuals had two cardiovascular risk factors, while the remaining twelve individuals had one cardiovascular risk factors (▶Tab. 1). The mean Framigham Risk Score (FRS) in the cardiovascular risk and control group was 18±15 and 4±5, respectively. Although total plasma cholesterol, triglyceride and glucose levels were within normal range in the cardiovascular risk and control group, they were significantly higher in cardiovascular risk individuals. LDL cholesterol levels were higher in cardiovascular risk than

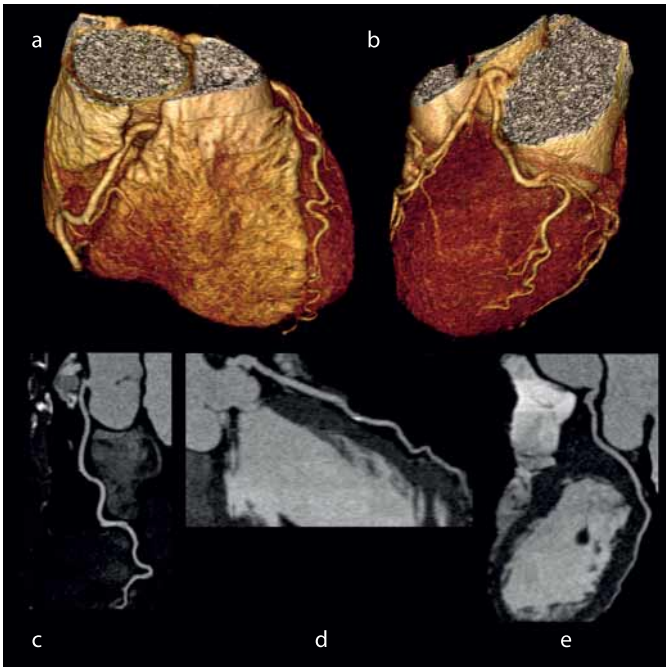

Fig. 1 ECG-pulsing CT angiography using the ECG-dependent dose modulation in a 42 year old individual with borderline hypercholesterolemia
a, b) Volume-rendered image illustrates right coronary artery (left panel) and the left coronary arteries (right panel) without evidence of stenosis.
c) curved multiplanar 2D-reconstruction of the right coronary artery without evidence of stenosis; **d)** left anterior descending artery with a mild regional calcification in the middle segment; **e)** left circumflex artery without any stenosis

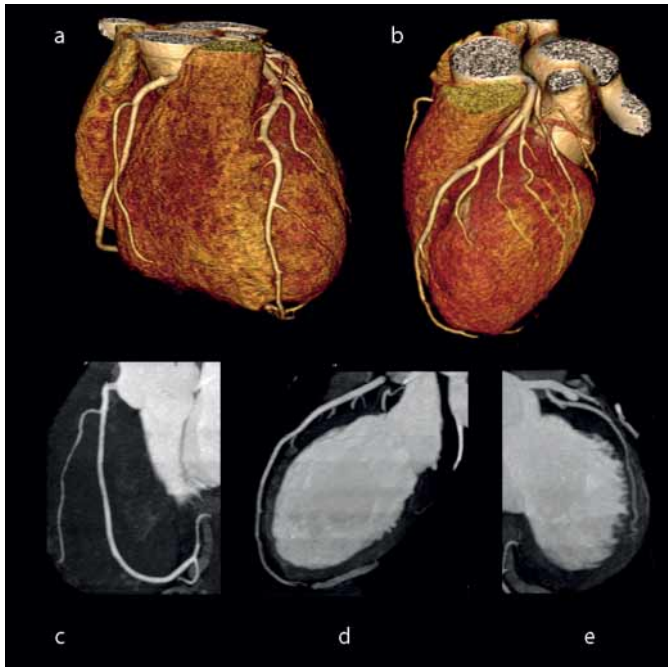

Fig. 2 Conventional helical CT angiography
a, b) Volume-rendered images demonstrate the right coronary artery (left panel) and the left coronary arteries (right panel) without evidence of stenosis.
c) curved multiplanar 2D-reconstruction of the right coronary artery
d) left anterior descending artery
e) left circumflex artery without any stenosis

in the control group without reaching statistically significance, while HDL cholesterol levels were non-significantly higher in the control group. ECG-pulsing CTA demonstrated normal coronary morphology in all individuals of the control group. Conversely, in the cardiovascular risk group, one individual had calcified plaque burden with luminal epicardial narrowing <50% in the LAD, RCA and LM, while there were two individuals with calcified plaque and stenosis ≥ 50% (first: LCx, and second: LAD and RCA). Further, in four cardiovascular risk individuals mild calcification without evidence for subintimal plaque burden was observed in the LAD artery (▶Fig. 1).

As regards the conventional helical CTA group with a intermediate-to-high pretest probability of CAD, these patients had more cardiovascular risk factors (6 with one, 4 with two and 6 with three cardiovascular risk factors) (▶Tab. 1). Total plasma cholesterol, LDL cholesterol, glucose and triglyceride levels were significantly higher than in the control group, while HDL-levels tended to be lower. Conventional helical CTA in this group (▶Fig. 2) demonstrated calcified plaque burden with stenosis <50% in four patients (LAD: 4, LCx: 1, RCA: 1) and calcified plaque burden with stenosis ≥ 50% also in four patients (LAD: 3, LCX: 2 and RCA: 2). In three patients of the conventional helical CTA group, there was moderate-to severe calcification with subsequent occlusion of the LCx. Further, in two patients of this group, minor calcifications without evidence for plaque burden on CTA were identified in the LAD, LCX and RCA, respectively. Finally, in nine individuals of the ECG-pulsing CTA "stair-step" artifacts of the epicardial artery due to patient movement or varying heart rate were noted in the LAD (n = 2), LCx (n = 4), and RCA (n = 5), while in the conventional helical CTA group it was observed in twelve individuals in the LAD (n = 7), LCx (n = 4), and RCA (n = 10). These "stair-step" artifacts could be compensated by adapting to image acquisition to the proper x-ray window of the RR cycle.

MBF measurements and radiation exposure

At rest, heart rate, systolic blood pressure and RPPs tended to be higher in cardiovascular risk individuals than in controls (▶Tab. 1). Similarly, PET-determined resting MBF was significantly higher in the cardiovascular risk group when compared to controls. During dipyridamole-stimulation of hyperemic flow increases, heart rates had increased significantly from rest, while they did not differ significantly between both groups (▶Tab. 1). Further, systolic blood pressure had significantly declined in cardiovascular risk individuals from rest, while it widely remained unchanged in controls. As denoted in ▶Table 1, hyperemic MBFs during dipyridamole-stimulation were significantly lower in the cardiovascular risk group than in controls (▶Fig. 3). When the hyperemic MBFs were related to the mean arterial blood pressure in order to account for possible interindividual differences in coronary driving

pressure, the resulting estimates of coronary vascular resistance (CVR) was higher in cardiovascular risk individuals as compared to controls (▶Tab. 1). In addition, the MFR was significantly lower in cardiovascular risk individuals than in controls. When an abnormal MFR was defined as ≤2.0, then 13 out of 16 (81%) in the cardiovascular risk group had an abnormal MFR, suggestive of coronary circulatory dysfunction, while in the control group a MFR of ≤2.0 was observed in one individual. As regards those cardiovascular risk individual without coronary plaque or calcification as evidenced by CTA, seven out of nine (78%) had an abnormally reduced MFR.

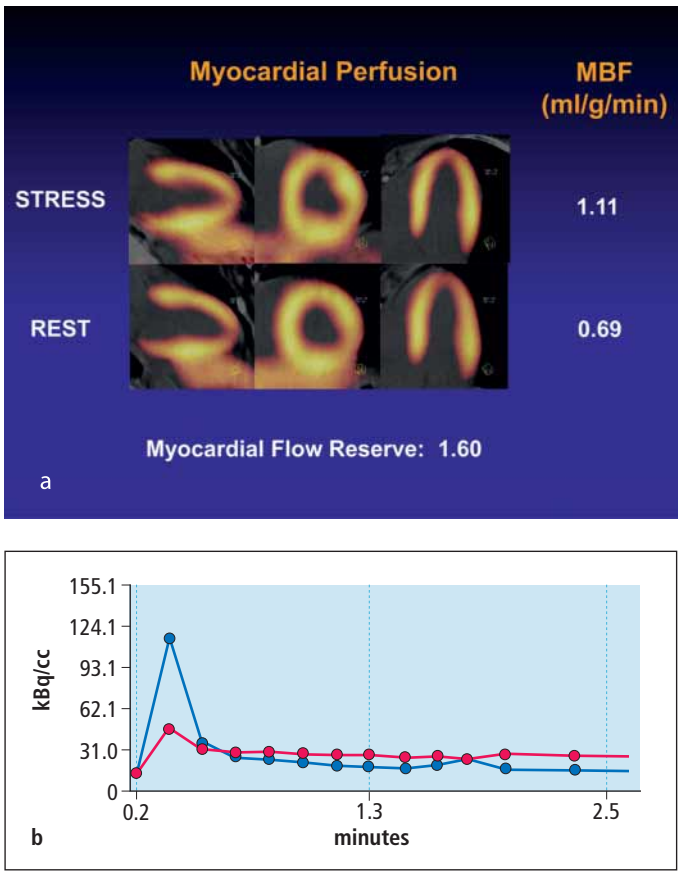

Fig. 3 ^{13}N-ammonia PET/CT: In this cardiovascular risk individual, MBF quantification with PET and a two-compartment tracer-kinetic model calculates a resting flow of 0.69 ml/g/min, while the hyperemic MBF increase during dipyridamole-stimulation of 1.11 ml/g/min is markedly reduced. In addition, the corresponding myocardial flow reserve (MFR= MBF during hyperemia/ MBF at rest) with 1.60 is abnormally low (reference > 2.5), which signifies coronary circulatory dysfunction as possible functional precursor of CAD. In view of the mild calcification in the mid LAD and the markedly reduced MFR of 1.6 preventive medical intervention with lipid-lowering treatment using a statin was installed.
a) Corresponding stress and rest myocardial perfusion study in the 42 year old borderline hypercholesterolemic person without flow-limiting epicardial lesions but with a mild calcified plaque in the mid LAD on ECG-pulsing CTA as denoted in Figure 1. The myocardial display demonstrates a homogenous ^{13}N-ammonia of the left ventricle during hyperemic flow stimulation with dipyridamole and at rest (midventricular vertical-, short-, and horizontal axis).
b) arterial radiotracer input function and myocardial tissue response: From regions of interest assigned to the left ventricular blood pool and left ventricular myocardium on the serially acquired images, time activity curves are derived that denote the alterations in radiotracer activity (y-axis) in the arterial blood pool (counts/pixel/second) and in the myocardium (counts/pixel/second) as a function of time (x-axis). Through fitting of the time activity curves with the operational equation formulated from tracer-kinetic models, myocardial blood flows are obtained in ml/g/min. The blue line denotes the arterial radiotracer input function, and the red line the myocardial tissue response.

Further, we evaluated a possible association between the Framingham Risk Score (FRS) and the hyperemic MBF during pharmacologic vasodilation. For the whole study group, the hyperemic MBF and the MFR significantly correlated with the FRS, respectively ($r = -0.60$, SEE = 0.46 and $p<0.001$; and $r = -0.50$, SEE = 0.92 and $p<0.01$). When only cardiovascular risk individuals were evaluated, there was also a correlation between the hyperemic MBF and the FRS ($r = -0.55$, SEE = 0.25 and $p<0.03$), while the association between the MFR and the FRS did not reach statistical significance ($r = -0.23$, SEE = 0.38 and $p = 0.39$).

The mean effect radiation dose of rest-stress ^{13}N-ammonia PET/CT perfusion study in the whole study population was 3.07±0.06 mSv (2.07±0.06 mSv from the stress-rest ^{13}N-ammonia injections, 1.0 mSv from the 2 CT transmission scans). As regards the mean effect radiation dose of the rest-stress ^{13}N-ammonia PET/CT perfusion study, it was similar in the control and cardiovascular risk group (3.04±0.04 vs. 3.06±0.04 mSv).

CTA and radiation exposure

After the assessment of myocardial perfusion and MBF quantification with ^{13}N-ammonia PET, coronary morphology with ECG-pulsing CTA was performed in twenty-six individuals as aforementioned (▶Tab. 1, ▶Tab. 2). Further, sixteen patients with intermediate-to-high probability of CAD underwent conventional helical CTA without PET assessment of myocardial perfusion. As can be appreciated in ▶Table 2, heart rate and body mass index (BMI) were comparable between patients undergoing ECG-pulsing CTA or conventional helical CTA. Dosimetric findings associated with the two CTA scanning protocol employed in the current study are denoted in ▶Table 3. As it was observed, $CTDI_{vol}$ and DLP were significantly lower with ECG-pulsing CTA than with conventional helical CTA. Further, the mean ED with ECG-pulsing CTA was only 5.5±2.0 mSv as compared to conventional helical CTA with 19.3±2.0 mSv ($p < 0.0001$). Thus, using ECG-pulsing technique reduced the radiation dose by 71.5% when compared to conventional helical CTA.

CTA image quality assessment

Image quality scores assigned to each coronary artery, along with the cumulative findings for all segments are demonstrated in ▶Table 4. ECG-pulsing CTA was performed in twenty-six individuals but three examinations were not included in the analysis of image quality because of severe motion artifacts (6 cases) and severe and diffuse coronary calcifications (2 cases). In the remaining eighteen individuals, a total of 231 coronary artery segments were evaluated (of 288 possible segments, 57 were excluded because of diameter < 1.5 mm or anatomical variant). Herefrom, 213 segments (92 %) were of diagnostic image quality (score 1–3): 117 segments (51%) with excellent image quality (score 1), 68 segments (29%) with mild blurring of the vessel wall (score 2) and 28 (12%) with moderate blurring of the vessel wall (score 3). Non-diagnostic image quality (score 4–5) was found in 18 segments (8%) (score 4 in 6 segments (3%) and score 5 in 12 segments (5%). In the comparative group of sixteen patients examined with conventional helical CTA, 188 coronary artery segments were evaluated (of 255 possible segments) and 167 segments (89%) were of diagnostic image quality (score 1–3): 83 segments (44 %) with excellent image quality (score 1), 43 segments (23%) with mild blurring of the vessel wall (score 2) and 42 (22%) with moderate blurring of the vessel wall (score 3). Non-diagnostic image quality (score 4–5) was found in 20 segments (11%) (score 4 in 15 segments (8%) and score 5 in 5 segments (3%).

The mean number of evaluable segments per patient in the group undergoing ECG-pulsing CTA was 12.8±1.7, which did not differ significantly from that of conventional helical CTA with 11.7±2.5 segments. For the overall coronary segment image quality on a five-point scale, no significant difference between ECG-pulsing CTA and conventional helical CTA was observed (1.8±1.2 vs 2.0±1.0) when the best reconstructed phase was considered. For the total number of segments, the image quality score was comparable between both CTA protocols; however, in LCx, more segments were considered not evaluable in conventional helical CTA group compared to ECG-pulsing CTA group (18% vs 3%, p= 0.005) due to anatomical variants, motion artifacts, and moderate-to-severe calcifications. Overall, however, non-diagnostic CTA image quality was comparable between ECG-pulsing CTA and conventional CTA (8% vs 11%).

Tab. 2 Comparison

computed tomography angiography (CTA)	ECG-pulsing	conventional helical
sex (women/men)	8/18	6/10
age (years)	52±17	59±11
body mass index (kg/m^2)	24±3	25±3
heart rate at rest (bpm)	61±7	58±7

p = NS between groups

Tab. 3 Radiation dose for the two scanning protocols

CTA	ECG-pulsing		conventional helical	
	mean±SD	range	mean±SD	range
$CTDI_{vol}$ (mGy)	18±6	11.8–29.1	69±1*	67.05–72.29
dose-length product (mGy cm)	328±117	201–588	1136±122*	905–1308
effective dose (mSv)	5.5±2	3.6–9.9	19.3±2*	15.3–22.2

*p < 0.0001 versus ECG-pulsing CTA; $CTDI_{vol}$: volume computed tomography dose index

Tab. 4 Image quality score for the two scanning protocols

image quality score		percentage of coronary segments		p
		ECG-pulsing CTA	conventional helical CTA	
all segments	1	51 (117/231)	44 (83/188)	0.242
	2	29 (68/231)	23 (43/188)	
	3	12 (28/231)	22 (42/188)	
	not evaluable†	8 (18/231)	11 (20/188)	
RCA	1	39 (26/66)	45 (24/53)	0.109
	2	26 (17/66)	13 (7/53)	
	3	21 (14/66)	38 (20/53)	
	not evaluable†	14 (9/66)	4 (2/53)	
LAD	1	55 (55/100)	48 (40/84)	0.589
	2	33 (33/100)	30 (25/84)	
	3	5 (5/100)	12 (10/84)	
	not evaluable†	7 (7/100)	10 (9/84)	
LCX	1	55 (36/65)	37 (19/51)	0.005
	2	28 (18/65)	22 (11/51)	
	3	14 (9/65)	23 (12/51)	
	not evaluable†	3 (2/65)	18 (9/51)	

Data within parentheses are raw data used to calculate percentages.
† Due to small dimension or missing data due to anatomic variants.

Discussion

These preliminary data indicate the feasibility of the suggested ^{13}N-ammonia PET/CT protocol for a combined evaluation of both myocardial perfusion, MBF and coronary morphology in the identification of subclinical CAD with a mean radiation exposure of 8.0 ± 1.5 mSv. This radiation exposure was comparable to conventional cardiac ^{99m}Tc-SPECT commonly associated with a radiation exposure ranging between 5–11.0 mSv depending on a one- or two-days study protocol (18, 19). Using "ECG-pulsing" technique reduced the radiation dose by ≈71% when compared to conventional helical CTA, while maintaining image quality of the coronary segments. The use of the ECG-pulsing technique for CTA, as suggested by the current and other recent investigations (9, 20), may afford a more widespread clinical use of PET and CTA in hybrid imaging protocols in the identification of subclinical stages and clinically manifest CAD.

The current study is unique in that myocardial perfusion, MBF and coronary morphology were evaluated in a one study session with the use of a hybrid PET/CT system. This is in agreement with recent observations (1, 11), assessing myocardial perfusion with ^{82}Rb or ^{15}O-water PET/CT and coronary morphology with low-dose CTA using a "step-and-shot" technique, but extend the latter findings to a hybrid PET/CT system using the blood flow agent ^{13}N-ammonia and ECG-pulsing CTA. Our suggested CTA protocol with ECG-pulsing triggered tube current modulation during a spiral scan appears to be scientifically sound as many manufacturers do not necessarily offer a CT sub-system that allows other techniques such as a sequential scanning with prospective ECG triggering ("step-and-shoot") (1, 10, 21–23). In particular, the CTA performed with ECG-pulsing in the current study yielded a relatively low mean dose of radiation exposure of 5.5 ± 2.0 mSv when compared to the use of conventional helical CTA with a mean radiation exposure of 19.3 ± 2.0 mSv. Conventional helical CTA protocols with retrospective ECG gating are commonly associated with a relatively high radiation exposure raging from 9.4 to 21.4 mSv (9, 15, 20). As shown recently, however, introducing a prospective ECG-gating protocol may reduce the total radiation dose down to 2.1 mSv (10, 24). Also, a direct head-to-head comparison of the total effective radiation doses between two CTA protocols demonstrated a 79% radiation decrease with retrospective as compared to prospective ECG-gating (20 mSv to 4.1 mSv) (25). This agrees with the current comparative CTA evaluation between "ECG-pulsing" CTA and conventional helical CTA, which resulted in a 71% reduction in radiation exposure with the "ECG-pulsing" technique. As observed in the current study with ECG-pulsing CTA and previous investigations with prospective ECG-gating CTA (10, 25–27), despite a substantial reduction in radiation dose, the image quality could be maintained as compared to the conventional helical CTA. Notably, preliminary results non-obese patients suggests that, if a dual-source CT system is available, prospectively electrocardiogram-triggered high-pitch spiral CTA acquisition may be associated with a mean effective radiation dose of only 0.87 ± 0.07 mSv without a loss of image quality (28).

Helical CTA with ECG-pulsing in the current study was not only associated with a low radiation exposure but also allowed to compensate for so called "stair-step" artifacts of the epicardial artery in nine individuals. Such artifacts may occur due to misalignment of two adjacent data sets caused by patient movement, obese patients, or varying heart rate during image acquisition. In CTA with prospective ECG-gating and a very small x-ray window at only 75% of the RR cycle, as commonly used for the snap-shot pulse sequence (1, 10, 22, 24), patient movement or varying heart rate will lead to image acquisition in slightly different phases of the cardiac cycle causing stair-step artifacts of the vessels. In this regard, tube current modulation according to the ECG during a spiral scan affords the advantage of image acquisition during a greater x-ray window between 65–75% of the of the RR cycle. While in the current study this allowed corrections of some stair-step artifacts and, thereby, improved the diagnostic quality of the ECG-pulsing CTA, it was associated with a mildly higher mean radiation radiation burden of 5.5 mSv as compared to 2 mSv as reported more recently for prospective ECG-gating with snap-shot pulse sequence (10, 24).

Regarding the blood flow agents ^{13}N-ammonia and ^{82}Rb in the assessment of myocardial perfusion with PET imaging, ^{13}N-ammonia offers the advantage of a lower radiation exposure of ≈2 mSv as compared to commonly reported 5–12 mSv for rest-stress rubidium-82 PET perfusion studies (29, 30). The overall radiation exposure of the ^{13}N-ammonia PET/CT and CTA exam in the evaluation of both myocardial perfusion and coronary morphology was in the mean 8.0 ± 1.5 mSv, that compares well to the conventional assessment of myocardial perfusion with ^{99m}Tc-SPECT associated with a radiation exposure ranging between 5–11 mSv (15, 18, 19, 31–33), or ^{82}Rb PET/CT perfusion imaging with a mean effective dose of 13.8 mSv (18, 29). In particular, the radiation exposure of about 8.0 ± 1.5 mSv for the combined assessment of myocardial perfusion and coronary morphology with ^{13}N-ammonia PET/CT and ECG-pulsing CTA in the current study was substantially lower than to ≈20 mSv for hybrid imaging with ^{99m}Tc-SPECT and CT-angiography or to ≈27 mSv of dual-isotope (^{201}Tl/^{99m}Tc) SPECT perfusion imaging (18).

More recently, the increasing installation of hybrid PET/CT scanners has enabled an improved identification of flow-limiting CAD in women and obese patients, who are commonly prone to attenuation artifacts with conventional SPECT perfusion imaging. As it has been shown (29), using ^{82}Rb PET with CT-based attenuation correction may yield a high sensitivity for detecting CAD of 95%, a specifity of 83%, and diagnostic accuracy of 87% in women and obese patients. In view of the epidemic of obesity in the industrialized countries (29, 34), an increasing use of PET/CT scanners with an optimal CT-based attenuation correction for the assessment of myocardial perfusion in obese patients is likely, resulting in an optimized diagnostic accuracy of the CAD process in these patients. The current study provides an important estimate of a relatively low mean effective radiation exposure of 8.0 ± 1.5 mSv for ^{13}N-ammonia PET/CT and ECG-pulsing

CTA in the combined assessment of myocardial perfusion and coronary morphology. As there is an ongoing and rapid development of PET/CT and also of SPECT instrumentation (35–37), substantially lower radiation exposure can be expected in the near future. The latter is likely to allow a more widespread use of the combined assessment of myocardial perfusion and coronary morphology with PET/CT hybrid systems or separate use of SPECT, PET and CT-systems with fusion imaging techniques (22, 36).

Another important aspect is that PET imaging does not only afford the visual and semiquantitative assessment of myocardial perfusion in the detection of flow-limiting epicardial disease but also the concurrent evaluation of regional MBF of the left ventricle in absolute terms (ml/min/g) (3, 38, 39). This enables the assessment of the MBF at rest and during pharmacologic vasodilation with the resulting myocardial flow reserve and, thereby, enables the identification and characterization of an impairment of coronary circulatory dysfunction in cardiovascular risk individuals as a functional precursor of developing CAD (3,39). Such abnormalities in coronary circulatory function may not only parallel but they may also precede atherosclerotic disease-related structural alterations of the epicardial artery as observed in previous investigations (40). This is in line with the current observation that 78% of cardiovascular risk individuals had normal CTA but abnormally reduced MFRs. In contrast, all cardiovascular risk individuals with some mild calcified or non-calcified plaque burden on CTA also presented a diminished MFR. Thus, in the current small cardiovascular risk population, the presence of calcified and non-calcified coronary plaque burden was accompanied by a diminished response of hyperemic flows. This may accord with the consideration that the integrity of coronary circulatory function reflects a pivotal factor in counterbalancing the initiation and progression of the CAD process (7,39). According to this, the magnitude of coronary flow increase during times of increased metabolic demand defines the amount of flow-mediated and, thus, endothelium-dependent release of atheroprotective nitric oxide of the coronary circulation (3,7). In patients with normal PET or SPECT myocardial perfusion imaging, the identification of coronary plaque burden by CTA therefore may not only signify a subclinical CAD process but also a diminished function of the coronary circulation. Conversely, the magnitude of hyperemic MBFs in individuals with a similar degree of CAC may vary considerably (3, 41). Thus, the detection of mild coronary plaque burden on CTA may not necessarily be associated with abnormally reduced hyperemic MBFs in the individual.

Interestingly, as observed in the current and in previous investigations (42), in asymptomatic individuals with a low to intermediate Framingham risk, the PET-measured hyperemic MBFs and the MFR inversely correlated with the estimated 10-year coronary heart disease risk, while a considerable variability in the extent of hyperemic MBFs was observed. In this direction, the identification of PET-measured reductions in hyperemic MBFs or MFR in asymptomatic individuals at low or moderate cardiovascular risk could aid in the identification of those individuals who are in fact at higher cardiovascular risk (42, 43), and who could benefit from the installation or re-enforcement of preventive medical treatment (3), which, however, needs to be proven in future large scale clinical endpoint trials. The assessment of myocardial flow and coronary morphology with PET/CT hybrid imaging techniques, however, may be a unique approach to optimize the coronary risk stratification in cardiovascular risk individuals and to guide preventive medical intervention. The substantial lower radiation exposure of the current ECG-pulsing CTA technique in conjunction with ^{13}N-ammonia PET may reflect another important step towards a comprehensive evaluation of myocardial perfusion and coronary morphology with PET/CT in the identification of subclinical and clinically manifest CAD process.

Conclusion

These preliminary data emphasize the feasibility of the suggested ^{13}N-ammonia PET/CT protocol for a combined evaluation of both myocardial perfusion and coronary morphology in the identification of subclinical CAD with a relatively low mean radiation exposure of 8.0 ± 1.5 mSv. This low-dose ^{13}N-ammonia PET/CT protocol compares well to the radiation exposure of conventional ^{99m}Tc-SPECT with 5–11 mSv and, thus, may allow the evaluation not only of myocardial perfusion but also of coronary morphology in a single cardiac examination.

Acknowledgement

This work was supported by the Swiss National Science Foundation (SNF grant: 3200B0–122237), by a Clinical Research Grant of the Department of Internal Medecine of the University Hospitals of Geneva (Switzerland), and by a Atherothrombosis Research Fellowship Grant for Dr. G. Vincenti from the European Society of Cardiology (ESC) and by a Fellowship Grant from the Italian Society of Cardiology (Societa Italiana di Cardiologia; SIC).

Conflict of interest

The authors declare, that no potential conflict of interest exists and all sources of funding for the work are acknowledged.

References

1. Javadi M, Mahesh M, McBride G et al. Lowering radiation dose for integrated assessment of coronary morphology and physiology: first experience with step-and-shoot CT angiography in a rubidium 82 PET-CT protocol. J Nucl Cardiol 2008; 15: 783–790.
2. Namdar M, Hany TF, Koepfli P et al. Integrated PET/CT for the assessment of coronary artery disease: a feasibility study. J Nucl Med 2005; 46: 930–935.
3. Schindler TH, Zhang XL, Vincenti G et al. Role of PET in the evaluation and understanding of coronary physiology. J Nucl Cardiol 2007; 14: 589–603.
4. Bengel FM, Higuchi T, Javadi MS, Lautamaki R. Cardiac positron emission tomography. J Am Coll Cardiol 2009; 54: 1–15.
5. Schelbert HR. Coronary circulatory function abnormalities in insulin resistance: insights from positron emission tomography. J Am Coll Cardiol 2009; 53: S3–8.
6. Van Werkhoven JM, Schuijf JD, Gaemperli O et al. Prognostic value of multislice computed tomography and gated single-photon emission computed tomography in patients with suspected coronary artery disease. J Am Coll Cardiol 2009; 53: 623–632.

7. Schindler TH, Nitzsche EU, Schelbert HR et al. Positron emission tomography-measured abnormal responses of myocardial blood flow to sympathetic stimulation are associated with the risk of developing cardiovascular events. J Am Coll Cardiol 2005; 45: 1505–1512.
8. Herzog BA, Husmann L, Valenta I et al. Long-term prognostic value of ^{13}N-ammonia myocardial perfusion positron emission tomography added value of coronary flow reserve. J Am Coll Cardiol 2009; 54: 150–156.
9. Hausleiter J, Meyer T, Hadamitzky M et al. Radiation dose estimates from cardiac multislice computed tomography in daily practice: impact of different scanning protocols on effective dose estimates. Circulation 2006; 113: 1305–1310.
10. Husmann L, Valenta I, Gaemperli O et al. Feasibility of low-dose coronary CT angiography: first experience with prospective ECG-gating. Eur Heart J 2008; 29: 191–197.
11. Kajander S, Ukkonen H, Sipila H et al. Low radiation dose imaging of myocardial perfusion and coronary angiography with a hybrid PET/CT scanner. Clin Physiol Funct Imaging 2009; 29: 81–88.
12. Grundy SM, Pasternak R, Greenland P et al. Assessment of cardiovascular risk by use of multiple-risk-factor assessment equations: a statement for healthcare professionals from the American Heart Association and the American College of Cardiology. Circulation 1999; 100: 1481–1492.
13. DeGrado TR, Hanson MW, Turkington TG et al. Estimation of myocardial blood flow for longitudinal studies with ^{13}N-labeled ammonia and positron emission tomography. J Nucl Cardiol 1996; 3: 494–507.
14. Koepfli P, Wyss CA, Namdar M et al. Beta-adrenergic blockade and myocardial perfusion in coronary artery disease: differential effects in stenotic versus remote myocardial segments. J Nucl Med 2004; 45: 1626–1631.
15. Einstein AJ, Moser KW, Thompson RC et al. Radiation dose to patients from cardiac diagnostic imaging. Circulation 2007; 116: 1290–305.
16. Radiation dose to patients from radiopharmaceuticals (Addendum 2 to ICRP Publication 53): ICRP Publication 80. Ann ICRP 1998; 28: 1–126.
17. Austen WG, Edwards JE, Frye RL et al. A reporting system on patients evaluated for coronary artery disease. Report of the Ad Hoc Committee for Grading of Coronary Artery Disease, Council on Cardiovascular Surgery, American Heart Association. Circulation 1975; 51: 5–40.
18. Thompson RC, Cullom SJ. Issues regarding radiation dosage of cardiac nuclear and radiography procedures. J Nucl Cardiol 2006; 13: 19–23.
19. Nosske D, Minkov V, Brix G. Establishment and application of diagnostic reference levels for nuclear medicine procedures in Germany. Nuklearmedizin 2004; 43: 79–84.
20. Hausleiter J, Meyer T, Hermann F et al. Estimated radiation dose associated with cardiac CT angiography. JAMA 2009; 301: 500–507.
21. Gaemperli O, Schepis T, Koepfli P et al. Accuracy of 64-slice CT angiography for the detection of functionally relevant coronary stenoses as assessed with myocardial perfusion SPECT. Eur J Nucl Med Mol Imaging 2007; 34: 1162–1171.
22. Pazhenkottil AP, Herzog BA, Husmann L et al. Noninvasive assessment of coronary artery disease with CT coronary angiography and SPECT: a novel dose-saving fast-track algorithm. Eur J Nucl Med Mol Imaging 2010; 37: 522–527.
23. Siegrist PT, Husmann L, Knabenhans M et al. ^{13}N-ammonia myocardial perfusion imaging with a PET/CT scanner: impact on clinical decision making and cost-effectiveness. Eur J Nucl Med Mol Imaging 2008; 35: 889–895.
24. Husmann L, Herzog BA, Gaemperli O et al. Diagnostic accuracy of computed tomography coronary angiography and evaluation of stress-only single-photon emission computed tomography/computed tomography hybrid imaging: comparison of prospective electrocardiogram-triggering vs. retrospective gating. Eur Heart J 2009; 30: 600–607.
25. Hirai N, Horiguchi J, Fujioka C et al. Prospective versus retrospective ECG-gated 64-detector coronary CT angiography: assessment of image quality, stenosis, and radiation dose. Radiology 2008; 248: 424–430.
26. Earls JP, Berman EL, Urban BA et al. Prospectively gated transverse coronary CT angiography versus retrospectively gated helical technique: improved image quality and reduced radiation dose. Radiology 2008; 246: 742–753.
27. Shuman WP, Branch KR, May JM et al. Prospective versus retrospective ECG gating for 64-detector CT of the coronary arteries: comparison of image quality and patient radiation dose. Radiology 2008; 248: 431–437.
28. Achenbach S, Marwan M, Ropers D et al. Coronary computed tomography angiography with a consistent dose below 1 mSv using prospectively electrocardiogram-triggered high-pitch spiral acquisition. Eur Heart J 2010; 31: 340–346.
29. Sampson UK, Dorbala S, Limaye A et al. Diagnostic accuracy of rubidium-82 myocardial perfusion imaging with hybrid positron emission tomography/computed tomography in the detection of coronary artery disease. J Am Coll Cardiol 2007; 49: 1052–1058.
30. Lautamaki R, George RT, Kitagawa K et al. Rubidium-82 PET-CT for quantitative assessment of myocardial blood flow: validation in a canine model of coronary artery stenosis. Eur J Nucl Med Mol Imaging 2009; 36: 576–586.
31. Lindner O, Burchert W, Bengel FM et al. Myocardial perfusion scintigraphy 2008 in Germany – Results of the fourth query. Nuklearmedizin 2010; 49: 65–72.
32. Lindner O, Burchert W, Bengel FM et al. Myocardial perfusion scintigraphy 2007 in Germany--results of the query and current status. Nuklearmedizin 2009; 48: 131–137.
33. Schäfers M, Bengel F, Büll U et al. Position paper nuclear cardiology: update 2008. Nuklearmedizin 2009; 48: 71–78.
34. Schindler TH, Cardenas J, Prior JO et al. Relationship between increasing body weight, insulin resistance, inflammation, adipocytokine leptin, and coronary circulatory function. J Am Coll Cardiol 2006; 47: 1188–1195.
35. Valenta I, Treyer V, Husmann L et al. New reconstruction algorithm allows shortened acquisition time for myocardial perfusion SPECT. Eur J Nucl Med Mol Imaging 2010; 37: 750–757.
36. Kaufmann PA. 82-Rubidium--the dawn of cardiac PET in Europe? Eur J Nucl Med Mol Imaging 2007; 34: 1963–1964.
37. Brown TL, Merrill J, Hill P, Bengel FM. Relationship of coronary calcium and myocardial perfusion in individuals with chest pain. Assessed by integrated rubidium-82 PET-CT. Nuklearmedizin 2008; 47: 255–260.
38. Schindler TH, Campisi R, Dorsey D et al. Effect of hormone replacement therapy on vasomotor function of the coronary microcirculation in post-menopausal women with medically treated cardiovascular risk factors. Eur Heart J 2009; 30: 978–986.
39. Schindler TH, Cadenas J, Facta AD et al. Improvement in coronary endothelial function is independently associated with a slowed progression of coronary artery calcification in type 2 diabetes mellitus. Eur Heart J 2009; 30: 3064–3073.
40. Schindler TH, Facta AD, Prior JO et al. Structural alterations of the coronary arterial wall are associated with myocardial flow heterogeneity in type 2 diabetes mellitus. Eur J Nucl Med Mol Imaging 2009; 36: 219–229.
41. Schindler TH, Zhang XL, Vincenti G et al. Diagnostic value of PET-measured heterogeneity in myocardial blood flows during cold pressor testing for the identification of coronary vasomotor dysfunction. J Nucl Cardiol 2007; 14: 688–697.
42. Dorbala S, Hassan A, Heinonen T et al. Coronary vasodilator reserve and Framingham risk scores in subjects at risk for coronary artery disease. J Nucl Cardiol 2006; 13: 761–767.
43. Graf S, Khorsand A, Gwechenberger M et al. Typical chest pain and normal coronary angiogram: cardiac risk factor analysis versus PET for detection of microvascular disease. J Nucl Med 2007; 48: 175–181.